Los Alamos National Laboratory is operated by the University of California for the United States Department of Energy under contract W-7405-ENG-36

Microquake Activity Associated with Underground Nuclear Testing at the Nevada Test Site

Los Alamos National Laboratory
Los Alamos, New Mexico 87545

Edited by Glenda Ponder and Marge Wilson, ESS Division

LA-8552-MS

UC-11
Issued: August 1983

Microquake Activity Associated with Underground Nuclear Testing at the Nevada Test Site

C. L. Edwards
M. D. Harper
T. A. Weaver
D. J. Cash
J. M. Ray
E. F. Homuth

Los Alamos National Laboratory
Los Alamos, New Mexico 87545

CONTENTS

FIGURES

TABLE

MICROQUAKE ACTIVITY ASSOCIATED WITH UNDERGROUND NUCLEAR TESTING AT THE NEVADA TEST SITE

by

C. L. Edwards, M. D. Harper, T. A. Weaver,
D. J. Cash, J. M. Ray, and E. F. Homuth

ABSTRACT

In the fall of 1976, the Los Alamos Close-In Seismic Network was added to the existing strong motion net deployed around each nuclear test conducted by Los Alamos. Six to ten stations, including both accelerometers and seismometers, are installed within a two-DOB (depth of burial) circle around SGZ (surface ground zero) and operated until the major portion of the microquake activity ceases, usually within 48 hours. Epicentral locations are determined and local magnitudes are calculated from event durations.

Four primary conclusions have been reached on the basis of the data analyzed to date: (1) major faults bounding the immediate site of a nuclear test confine the observed microquake activity to the structural block in which the test is conducted; (2) microquake epicenters are generally distributed around the cavity created by the nuclear test with the peak occurrence generally occurring about three cavity radii away from the working point; (3) magnitudes of locatable microquakes apparently distribute randomly over the entire region of activity; and (4) the microquake activity as a function of time appears to be controlled by the collapse phenomenology.

I. INTRODUCTION

A. Scope

The Los Alamos National Laboratory has operated a short-period seismograph network in the immediate vicinity of some 25 underground nuclear explosions conducted at the Nevada Test Site (NTS). Although the seismic network was originally operated to gather data on the seismological effects of the explosions as they pertain to containment of the explosion, the data have also provided a wealth of information useful in the study of verification of foreign nuclear tests. Local seismological studies utilizing the main explosion and the many aftershocks can reveal many details about underground fault breakage, geologic layering effects, water table effects, and collapse effects. Such studies may also determine the explosive and tectonic stress release (source functions) associated with an underground explosion, which should allow a better interpretation of the seismic signals observed teleseismically.

Although other investigators (Boucher et al., 1969; Ryall and Savage, 1969; Hamilton and Healy, 1969; Perret, 1971) have operated seismograph networks in the vicinity of underground explosions, we believe we have the only

catalog of close-in measurements on a large number of explosions. Several investigators have identified or discussed seismic events that originate near the cavity formed by an underground nuclear test (Brune and Pomeroy, 1963; Hamilton et al., 1969; Perret, 1971; Engdahl, 1972; Stauder, 1971). We have fielded on-site [usually within two depth-of-burial (DOB) radii] seismic networks on 25 Los Alamos events with yields ranging from < 20 kt to 150 kt and burial depths ranging from 180 m to 650 m. The medium in which these detonations occurred was either alluvium or volcanic tuff. From these explosions we have over 3500 hours of recorded data. This extensive set of very close-in measurements has not only provided data on stress release associated with an underground explosive detonation, but has also provided valuable information on seismic station deployment, data acquisition and recording techniques, and data handling and processing techniques.

Any study of explosion-induced seismicity must be able to handle the large numbers of aftershocks that are produced over an extended period of time. For example, it is possible that as many as 10 000 microquake aftershocks may occur in the region of the detonation during the following 3 or 4 days. The data acquisition system must operate continuously to record all of these microquakes. Techniques must therefore be developed and provided to accommodate the large data base produced by such monitoring. Los Alamos has, after much effort, developed those techniques and the expertise required to handle the data acquisition and analysis.

B. Purpose

The Los Alamos program to monitor and interpret the microquake activity at the NTS was initiated to obtain data relevant to studies on various aspects of the phenomenology of underground nuclear explosions. For these studies, the microseismic data would be combined with additional data, such as photography, ground motion studies, and drill hole information, that have been collected over the many years of underground testing. Phenomenology studies for which the microquake data can provide significant input include:

1. Collapse Phenomena. The collapse of an explosion-formed cavity can be divided into three main phases: the initiation of collapse; the propagation of collapse through various geologic media; and the termination of collapse, resulting in either a surface crater or a subsurface apical void. Many theories exist concerning the mechanisms associated with each of these three phases. The precise location of microquakes before and during collapse provides relevant information to all three. Details of the chimneying and subsidence are given by Houser (1969).

2. Stress Regime Around Underground Cavities. An important aspect of containment is the residual stress cage or "magic membrane" that is predicted by the various containment stress wave calculations. The magnitudes, stress drops, fault plane solutions, and locations of the microquakes detected postshot can provide significant contributions to the understanding of the existence and decay of the predicted stress cage.

3. Tectonic Stress Release. Over the many years of underground testing, questions have arisen concerning tectonic stress release, or "can explosions cause earthquakes?" The studies of microquake location, stress drop, etc., provide data on induced stress at distances greater than a few cavity radii from the working point (the position below ground zero at which

the device is detonated). Interpretation of these data, using the local and regional geologic structure, will allow some investigations of the impact of stress resulting from a detonation on the local stress field.

II. DESCRIPTION OF THE EXPERIMENTS

A. Instrumentation

The study of underground nuclear explosion-induced aftershocks is accomplished using a high-gain, short-period seismic network deployed on the surface in the vicinity of the explosion. In many ways the seismic network is similar to those used in conventional microquake studies. The main difference is that this network is deployed over a relatively small area because the earthquakes originate at shallow depths, usually less than 2 km. The network also must be able to record a wide range of earthquake magnitudes (from $M_L = -3$ to $M_L = 3$) and to handle as many as 500 aftershocks per hour.

The Los Alamos NTS aftershock network consists of the field seismic stations, the data telemetry system, and the data recording system. The basic network data acquisition system is shown in Fig. 1.

1. Field Seismic Stations. The field seismic stations are deployed in an array around the nuclear device emplacement hole. The array usually consists of 7 to 10 seismic stations deployed at different azimuthal directions and at distances as large as 2 DOB from the nuclear device emplacement hole or surface ground zero (SGZ) (Fig. 2). The array is weighted with most of the seismic stations being at distances of 1 DOB or less.

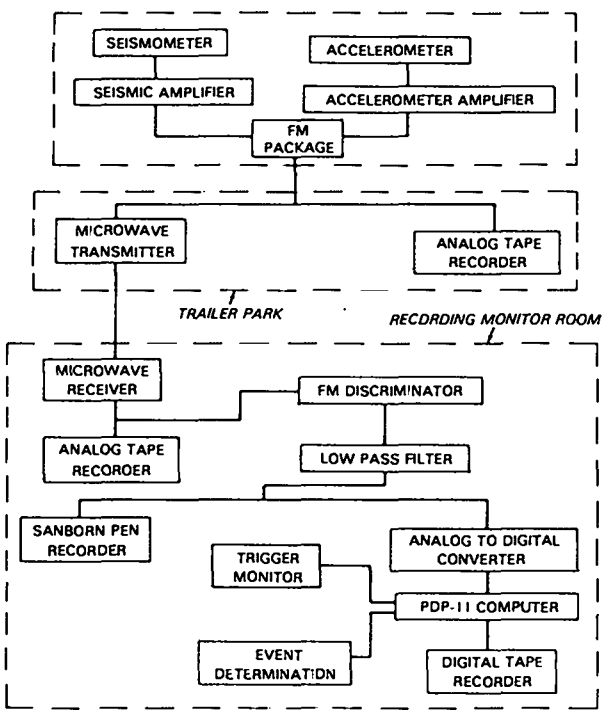

Fig. 1. Data acquisition system.

The seismic stations are operated at the maximum sensitivity allowable with the ambient noise present at NTS. Station magnifications (displacement) of between 150,000 and 600,000 at 10 Hz are typically obtained.

The seismic stations employ either a single vertical component seismometer (such as the Geospace HS-10 or the Mark Products L4-C) or a three-component seismometer (such as the Mark Products L4-3D) as the detector. All the seismometers have a natural frequency of 1 Hz and are operated at 70% damping for maximum flat response. The three-component seismometers are usually used at the stations most distant from the emplacement hole. The seismic stations frequently employ vertical or triaxial accelerometers (such as Endevco Model 2262-25G) to measure the strong ground motion signals produced at the time of detonation.

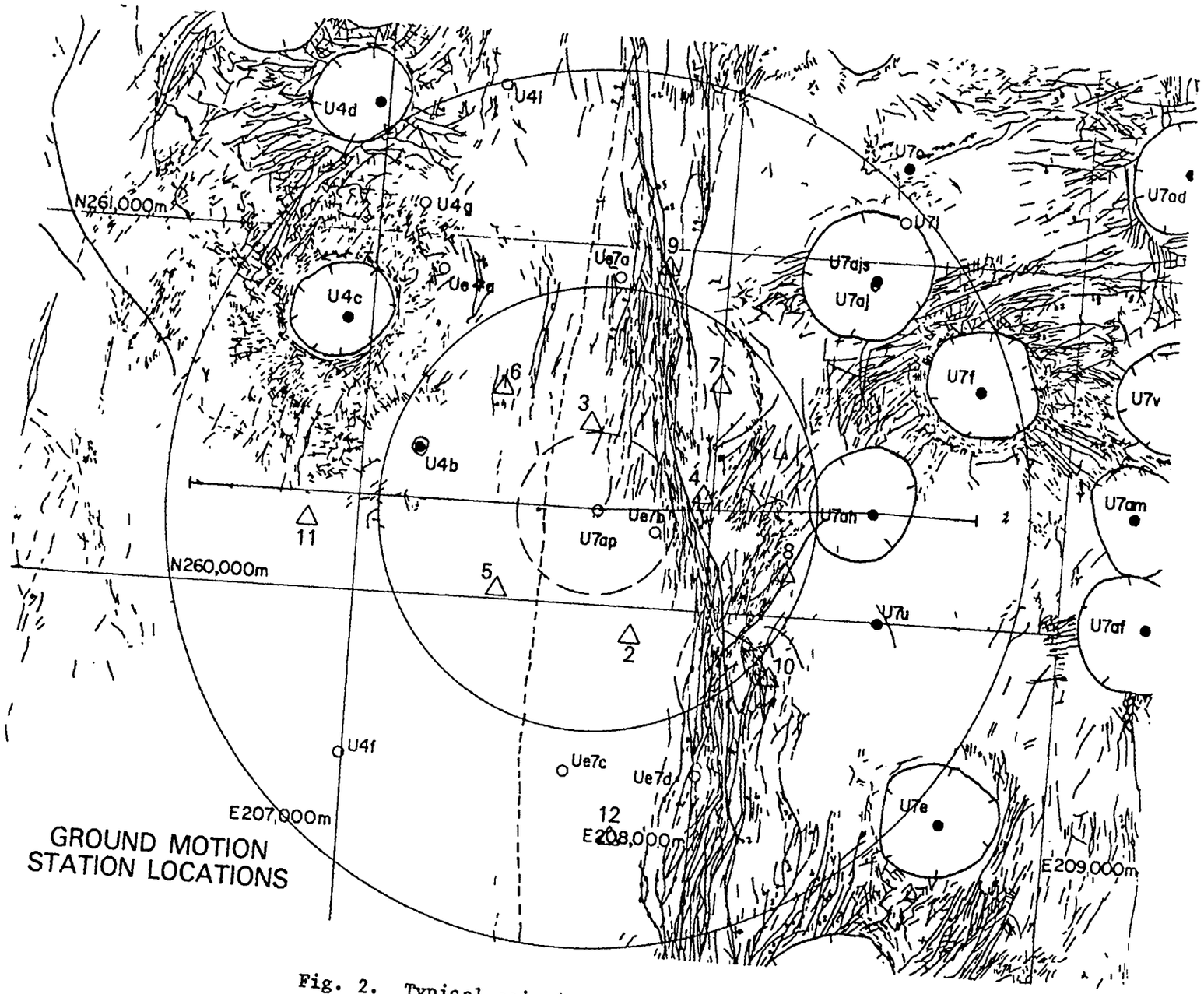

Fig. 2. Typical seismic station array.

The output signals from the seismometers are amplified up to 80 dB, low pass filtered at 100 Hz, and then applied to a voltage-controlled oscillator (VCO) in the FM package at each station. The various VCO signals are then mixed to form a composite signal for telemetry back to the recording site. The FM packages, which were designed and built by Los Alamos subcontractor EG&G, Inc., can each accept up to four channels of seismometer or accelerometer data. Usually a combination of both seismometer and accelerometer data is acquired at each seismic station.

2. Data Telemetry System. The composite VCO signals from the FM package at each seismic station are sent via coaxial cable to an instrumentation trailer that is located in the trailer complex where Los Alamos diagnostic measurements are taken. The cable runs between the instrumentation trailer and the seismic stations and are usually less than two DOB long. The coaxial cables also carry the power for the operation of the FM packages at each seismic station.

In the instrumentation trailer the signals are recorded on an analog, magnetic-tape recorder and also are transmitted, via microwave link, to the NTS Control Point, where they are recorded and processed. The analog recording done in the instrumentation trailer provides a backup recording system in case the microwave link fails during the strong ground motions created at detonation time.

3. Data Recording System. The composite signals, as received from the field instrumentation trailer via the microwave link, are recorded and undergo preliminary processing at the Laboratory Monitor Room in the Control Point complex. The equipment at the Laboratory Monitor Room consists of 14-channel analog tape recorders, timing systems synchronized to WWV time signals, signal conditioning electronics, a PDP-11/34 minicomputer and its associated peripheral equipment, and analog strip chart recorders.

The composite signals are recorded on the analog tape recorders to provide a permanent data file. These tape recorders operate continuously after the shot and produce an analog data tape every 13 hours.

To provide a more useful data set, the real time composite signals are discriminated, low pass filtered at 50 Hz, and then digitized at 200 samples per second. The digital data then undergo preliminary processing by the PDP-11 minicomputer. This processing produces a high-quality digital tape that contains only the data of interest.

These digitized data are then plotted by the Laboratory computer center in Los Alamos to produce film or paper records of the discrete seismic events. These records are analyzed by a data analyst to determine arrival times, first motions, and signal duration. It is at this point that a body of data useful for more detailed analyses such as hypocenter location, focal mechanism studies, etc., becomes available to the seismologist.

B. Analytical Methods

1. Microquake Hypocenter Estimation. The seismic data are analyzed and the estimated hypocenters of the microquakes are determined by a computer program, TODGE (The Over-Determined Gaussian Estimator). TODGE calculates the estimates of the hypocenter and origin time from the first arrivals of the seismic wave at an array of seismometers deployed on the surface of the ground. The seismic wave is assumed to propagate through a velocity medium

consisting of horizontal velocity layers of arbitrary number, thickness, and velocity. The description of the velocity layers is derived from the detailed geological and geophysical information available at the NTS. Then, by using an iterative, nonlinear optimization procedure, the estimates are determined such that the residual sum of squares between the observed and calculated travel times is a minimum.

Although a number of earthquake location procedures exist and are used extensively, the characteristics of the environment and the geophysical information utilized in these procedures are not adequate to be considered for the NTS microquake study. In normal earthquake location problems, distances of tens, hundreds, and thousands of kilometers are involved and most of the travel path of a seismic wave is in deeper, higher velocity layers, allowing a procedure to use travel time tables or a simple layered velocity model. However, the NTS microquakes occur within about a cubic kilometer, resulting in the need to consider travel paths through a multilayered velocity medium. Such detail could not be addressed by most of the models in literature.

2. Determination of the Velocity Model. Figure 3 shows the cross section through a typical site where a nuclear test was conducted. The cross section is constructed using geologic and geophysical data from the drill holes in the immediate area along with surface mapping and detailed surface gravity measurements. Although the geologic structure is quite complex, the velocity structure does not vary significantly over horizontal distances of a few hundred meters unless a major fault is encountered. Compressional velocities are measured in each hole drilled at the NTS. Within Areas 4 and 7 the velocity of a particular stratigraphic unit may vary by almost a factor of two, depending upon the thickness of the unit, the thickness of the overburden, and the local variation in composition. Table I shows this variation of velocity in the vicinity of drill hole U7av, using velocities measured, in U4f, U7au, U7aq to the west of the horst, U7ap, U7av, U7an in the horst, and in U7ah, Ue7zl, and U7ac to the east of the horst. The velocity model at U7av uses the velocity log measured in the drill hole. Below the bottom of the drill hole the layered velocity model is computed by using the geologic cross section and a relationship between the average velocity of a stratigraphic unit and its thickness and overburden. This relationship is derived empirically from velocity data taken from all drill holes in Areas 4 and 7. However, this velocity model is valid only for a few hundred meters around the drill hole. There may be significant variations in velocity across a fault and less significant variations within a dipping bed. The arrivals used to locate a microquake are normally only the arrivals at the

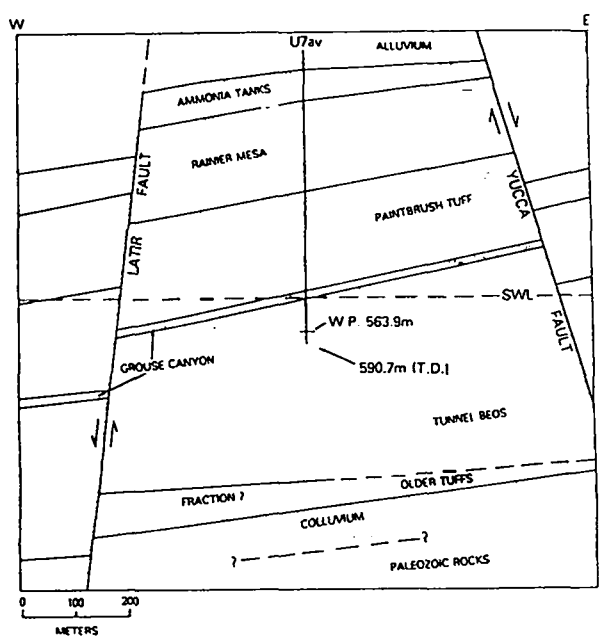

Fig. 3. East-west geologic cross section through LOWBALL--U7av.

TABLE I

MEASURED SEISMIC VELOCITIES (m/s) IN THE VICINITY OF U7au

Drill Hole	Geologic Unit				
	Qal (Alluvium)	Tma (Ammonia Tanks Tuffs)	Tmr (Rainier Mesa Tuffs)	Tp (Paintbrush Tuffs)	TT (Tunnel Bed Tuffs)
U4F	4380	6180	7950	8740	8930
U7au	4390	6250	8390	8590	7950
U7aq	4370	5770	9670	8860	8830
U7ap	3320	5030	6390	7470	7310
U7av	3290	4730	6750	7430	8280
U7an	3500	5120	7230	7700	8970
U7ah	3670	4070	6090	6630	8560
UE7Z1	4020	6470	7040	7440	8860
U7ac	3680	--	5930	6720	7830
Averages:					
West	4380	6070	8670	8730	8570
Central	3370	4960	6790	7530	8020
East	3790	5070	6350	6930	8420

closest stations, those within a few hundred meters; therefore, only a small portion of the travel path would be in an adjacent fault block. Microquakes within a few hundred meters of a nuclear test can be located quite accurately; however, to accurately locate events in adjacent fault blocks and at depths below the Paleozoic surface a more sophisticated velocity model will be required.

3. Station Corrections. Discrepancies have been observed between the measured and calculated travel times of the initial seismic wave from the nuclear explosion. These differences could be due to error in the velocity information, lateral inhomogeneity in the velocities because of structure, stratigraphy, etc., travel time anomalies attributed to the high energy source, other unknown phenomena, or a combination of these factors. To account for the errors at each seismometer station, a station correction was applied to the arrival time at each station. This forced the observed arrival times and the calculated arrival times from the velocity model to agree exactly for the nuclear explosion data.

Because the working point of the nuclear explosion and the positions of the seismometer stations were known, along with the time (fidu) of the explosion, the station corrections may be determined by taking the difference between the observed travel time of the seismic wave from the explosion to each station (which would be the arrival time at a particular station minus the fidu of the explosion) and the travel time calculated from the velocity model. The calculation of the travel times assumes a sonic wave travels through the medium according to the velocity information. However, the wave traveling from a nuclear explosion will initially travel in a supersonic manner for some distance and then travel the remaining distance in relation to the velocity information (Fig. 4).

The station corrections determined in this manner seemed to be superior to station corrections evaluated by ignoring the supersonic component of the travel time because the average correction was closer to zero and the magnitudes of the corrections were smaller. Although the difference between the two corrections was small in some cases, the change in the hypocenter estimates varied from small (20 m to 40 m) to significant (100 m to 200 m). Also, in some cases where an estimate was not found, convergence was obtained, yielding an estimated hypocenter.

4. Event Arrival Time Determination. The digital event tapes are used to produce record plots. The data analyst marks and measures the onset of the signal from each station. The first motion is noted, along with the duration of the event. The uncertainty in the pick times for a strong event is between 10 ms and 15 ms, while that for a weak event may be as large as 20 ms to 40 ms.

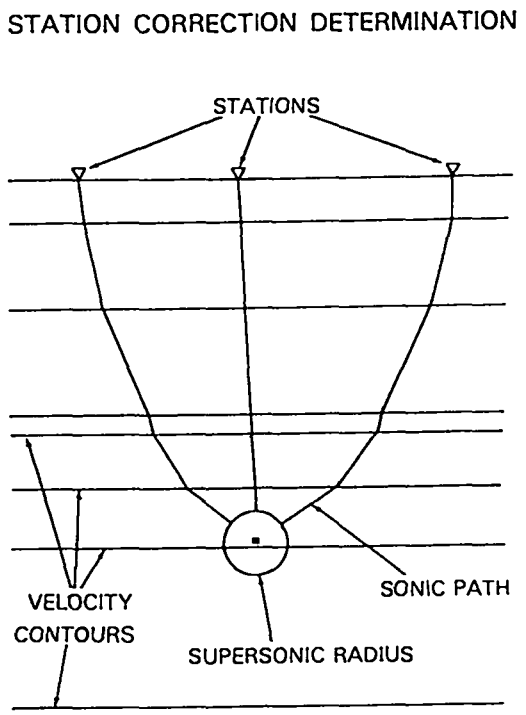

Fig. 4. Idealized seismic signal paths.

5. Error Analysis. A computer simulation was performed on the amount of error in the arrival times in an attempt to determine the corresponding amount of error in the final estimates from the model. The analysis proceeded in two phases. In the first phase we chose hypothetical event hypocenters and determined the travel times to each station using the velocity model, velocity information, and station locations for U7ap. Then, these times were perturbed randomly, events were located for these times using TODGE, and the amount of error was calculated between the hypothetical hypocenter and the new hypocenter estimated from the perturbed data. In the second phase we chose eight estimated hypocenters from the real data at U7ap. Then the same process was followed using the actual arrival times and the estimated hypocenters instead of the hypothetically determined ones.

In comparing the results from the hypothetical data and the actual data, a relationship between the error in the travel times and the error in the hypocenter estimates may be indicated. From picking times on the seismic traces, about 20 ms of error are assumed to exist. For a velocity of around 2000 m/s, the error in the pick time would correspond to 40-m error in distance. Thus, from 40 to 50 m of error is expected in the hypocenter estimates due to picking errors.

III. OBSERVED DATA AND ANALYSIS

A. U7ab - REDMUD

The U7ab site is located in east-central Area 7, 275 m west of the surface expression of the Area 7 Fault (Fig. 5). An additional fault, synthetic to the Area 7 Fault, has been assumed by projecting surface fractures southward. The distance to this fault, at its closest approach to the working point, is approximately 60 m. However, the projection of this fault is subject to a ±78-m error bar. The working point is located in the Tunnel Bed Tuffs, 385 m above the Paleozoic rock and about 105 m above the static water level. The cavity region average grain density is 2.39 g/cc and the average bulk density is 1.75 g/cc. The sink resulting from the event executed in U7ab is expressed at the surface by a shallow (approximately 2-m) depression. Slight reactivation of surface cracks occurred along a 400-m interval of the Area 7 Fault to the east and northeast. Minor discontinuous cracking appeared between 160 m and 400 m southeast of SGZ, but these features had no particular orientation. Well-defined fractures were present approximately 200 m southwest of SGZ and these fractures had a general north trend. The most prominent surface effects mapped were cracks strongly northwest-oriented and scattered throughout the northwest quadrant away from SGZ. These fractures extended from the perimeter fence to a distance of 350 m northwest of SGZ. Their dimensions ranged from short discontinuous cracks to fractures 80 m in length. None of the surface effects mapped had a residual vertical displacement.

Although there was some movement along the Area 7 Fault to the east and northeast, few of the microquakes located near the fault and none located to the east of the fault. Figure 5 shows the plan view of the U7ab site with the microquake epicenters. There are two clusters of events, one around SGZ and the other to the west-northwest of SGZ. Figure 6 shows the microquake hypocenters plotted on a cross section through the U7ab site. There is a cluster of shallow events near the pinch out of the Ammonia Tanks ash-flow tuff. There is another cluster of events in the bedded and ash-flow tuffs around the working point, apparently associated with the decay of the stress cage. Only a few events appear below the Crater Flat tuff. There are no located events in the chimney region above the cavity. There were only two events located to the east of the Area 7 Fault.

B. U7an - BILLET

The U7an emplacement hole lies within a structural horst bounded by the Latir Fault on the west and the Yucca Fault on the east (Fig. 7). The Latir Fault is not as well defined this far south but appears as a photo lineation. The emplacement hole was center-punched with a smaller diameter exploratory hole, which penetrated the Paleozoic colluvium. This provided good information on the relative position of the Paleozoic rock and the overlying stratigraphy. The U7an working point (635 m) was in the upper Tunnel Beds,

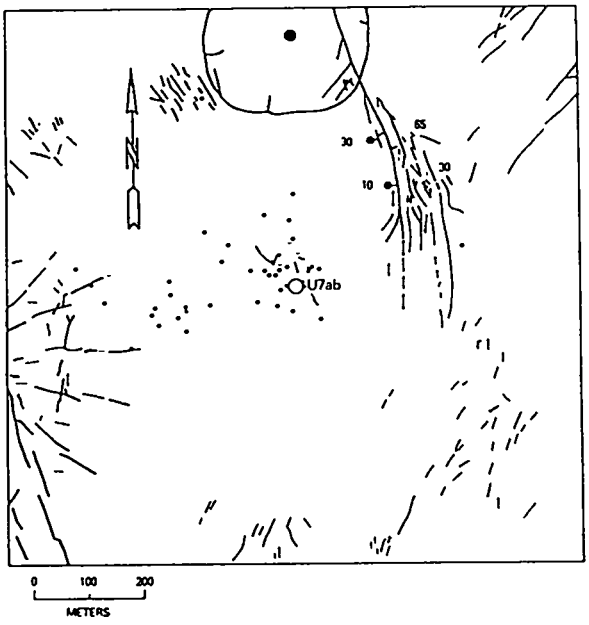

Fig. 5. Plan view--REDMUD--U7ab.

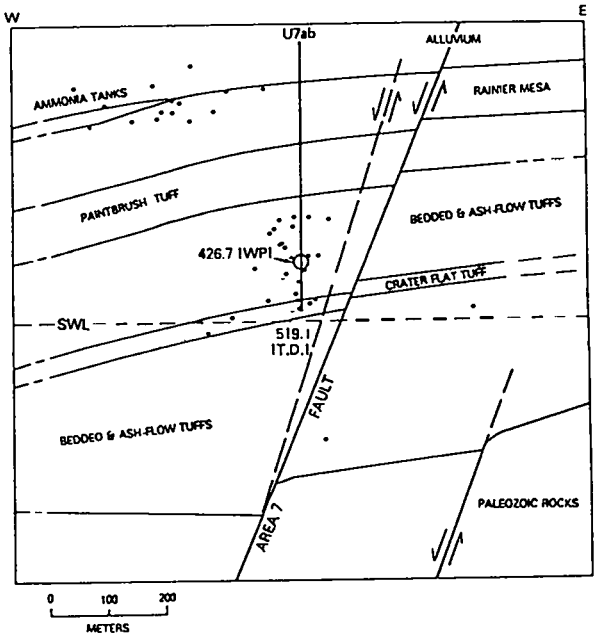

Fig. 6. Cross section--REDMUD--U7ab.

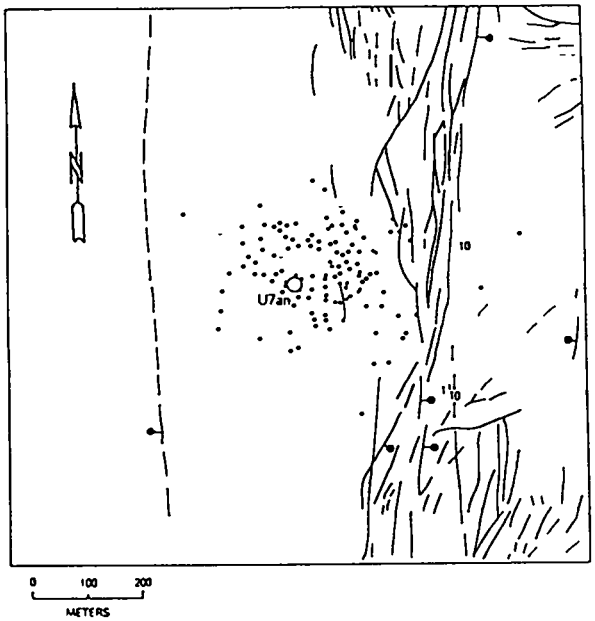

Fig. 7. Plan view--BILLET--U7an.

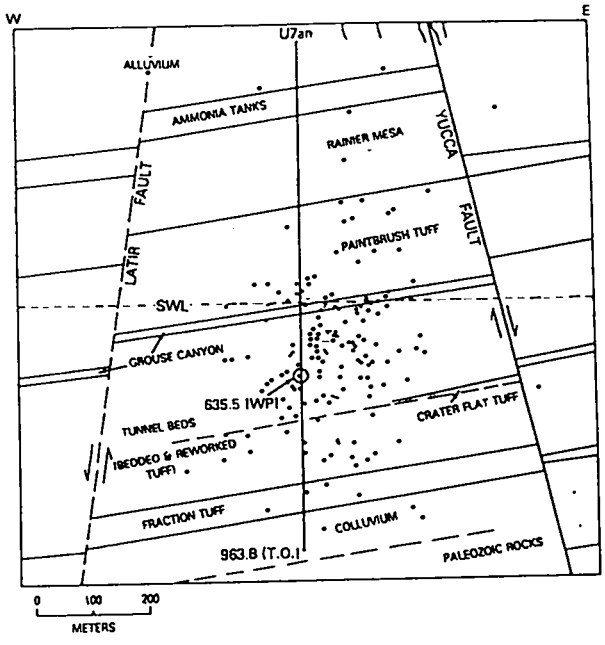

Fig. 8. Cross section--BILLET--U7an.

135 m below the static water level and 380 m above the Paleozoic colluvium. The nearest major structure is the Latir Fault, which passes about 335 m (±78 m) west of the working point at its closest approach. The U7an cavity region has an average grain density of 2.44 g/cc and an average bulk density of 1.84 g/cc. Since the U7an event was the first executed in this structural horst, the resulting surface effects were under considerable scrutiny. A surface sink did not occur and there was nearly a total absence of fracturing close to SGZ. There was major surface reactivation of cracks along the Yucca Fault with vertical displacements as much as 40 cm. Activation of surface cracks took place for a distance of over 2000 m along the Yucca Fault. Sets of cracks formed to the north and west of U7an, but these are generally discontinuous and isolated. Minor activation at the surface occurred for a distance of 500 m along the Latir Fault. However, this activation occurred well to the northwest, and there is a conspicuous absence of cracking along the Latir Fault's closest approach to U7an, due west of the SGZ. Although there was movement along the Yucca and Latir Faults, very few microquakes were located in the vicinity of either of these faults. Figure 7 shows the locations of the microquakes on the plan view of the U7an site. The majority of epicenters cluster to the northeast of SGZ. Figure 8 shows the microquake hypocenters located on the cross section through the U7an site. Note that very few hypocenters plot to the east of the Yucca Fault or to the west of the Latir Fault, that is, outside the structural block in which the test was conducted. There is a dense population of microquakes in the bedded tuffs around the working point. However, few events locate deeper in the section, below the tunnel beds. Only a few events were located in the vicinity of the Tuff-Paleozoic interface. There are also scattered shallow microquakes that could possibly be associated with the depth of spall. While microquakes do not appear to cluster along stratigraphic interfaces, several events do occur near the water table boundary. Few microquakes located in the chimney region above the cavity.

C. U7ap - CREWLINE

The U7ap drill hole is located near the north end of the same structural horst containing the U7av and U7an sites to the south (Fig. 9). The horst is well defined by the Latir Fault on the west, which passes approximately 325 m (±78 m) away from the working point. The east side of the horst is bounded by the Yucca Fault. The working point, at 564-m depth, lies within the Tunnel Beds, just above the Crater Flat tuff. This places it approximately 65 m below the static water level and 315 m above the Paleozoic rock. The cavity region averages are 2.51 g/cc for grain density and 1.97 g/cc for bulk density. These averages are slightly higher than the other two sites (U7av and U7an) in the horst and may be influenced by the presence of Crater Flat tuff in the lower cavity region. Postshot surface effects at the U7ap site are marked by the absence of a sink. Fracturing is generally distributed on all sides of the site with minimal cracking occurring due south of SGZ. Very little fracturing took place toward the Yucca Fault on the east. The event propagated prominent radial surface fractures in several azimuths away from SGZ, but they are particularly prominent toward the west and southwest. Significant information was obtained to further define the Latir Fault. Vertical displacement at the surface was mapped and is noted by a bar and ball placed on the downthrown block in Fig. 9. As the surface cracking along the fault approaches the U7ap site, both from the north and the south, it is captured by radial fractures and loses definition immediately west of the U7ap

site. West of the Latir Fault and the prominent radial fractures previously discussed, additional cracks occur and are decidely north-trending. These cracks are probably induced by slumping antithetical to the Latir Fault within the alluvium. Figure 9 shows the microquake epicenters plotted on a plan view of the U7ap site. Most of the events cluster around SGZ and within the structural block. Figure 10 shows the microquake hypocenter plotted on a cross section through the U7ap site. Very few of the microquakes locate along either the Latir or the Yucca Faults. No events locate outside the structural block in which the test was conducted. The events clustering around the cavity are somewhat diffuse and could be associated with the decay of the stress cage. The events that cluster along the Fraction Tuff-Paleozoic interface result from the interaction of the stress wave generated by the nuclear test and the impedance mismatch at the Tuff-Paleozoic boundary. Only a few events plot in the chimney region.

D. U7av - LOWBALL

The U7av emplacement hole is located in a structural horst in western Area 7 (Fig. 11). The horst is defined by the Latir Fault on the west and the Yucca Fault on the east. Both the Latir Fault and the Yucca Fault have surface expression in this region of Yucca Valley. The nearest major fault is the Latir Fault passing approximately 350 m ($\pm$78 m) to the west at its closest approach to the working point. The U7av working point, at 564 m, is in the Tunnel Beds, approximately 60 m below the static water level and 340 m above the Paleozoic rock. The U7av site is just north of U7an in the same structural horst. The average densities in the cavity region, 2.47 g/cc grain and 1.91 g/cc bulk, are similar to those found in U7an.

The U7av event resulted in the formation of a surface sink approximately 110 m in diameter and 23 m deep. Radial fractures concomitant with the Yucca Fault are well defined at the southeast perimeter. Other dominant radial patterns formed to the north and west of SGZ. Most of the radial patterns are interspersed with relatively short and discontinuous concentric fractures. Activation occurs along the surface expression of the Latir Fault to the west of the sink for a distance of about 300 m. Definition of the Latir Fault in this vicinity is enhanced because it lies in a concentric position relative to SGZ. No measurable residual vertical displacements were noted on either the Yucca or Latir Faults.

Although there was movement along the Latir Fault to the west and the Yucca Fault to the east at shot time, very few microquakes occurring later in time located near either fault. Figure 11 shows the plan view of the U7av site with the microquake epicenters located. Most of the microquake activity is confined to the structural block in which the nuclear test was conducted. More than half of the epicenters locate to the west of the drill hole. Figure 12 shows the cross section with the microquake hypocenters. Most of the microquakes cluster around the working point and are probably associated with the stress cage. Only a dozen microquakes are located along the Tuff-Paleozoic interface. Very few events are located in the chimney region or along the water table boundary.

IV. SUMMARY AND CONCLUSIONS

A. Effects of the Geologic Setting

The major faults bounding the site of a nuclear test appear to confine the events within the structural block in which the nuclear test was conducted.

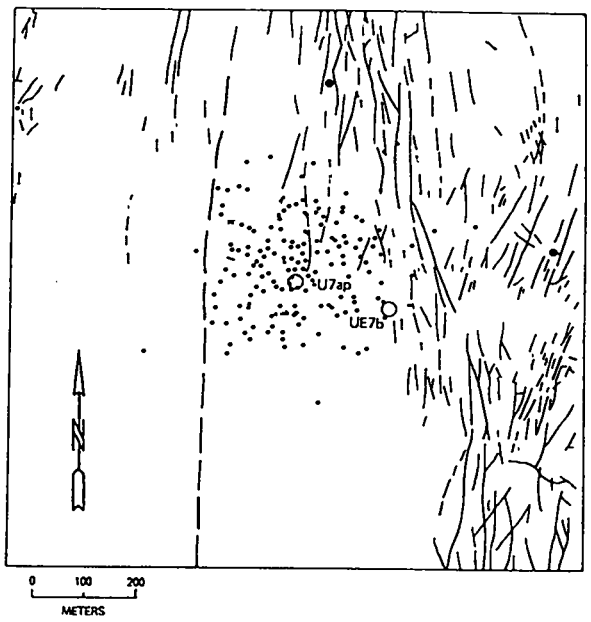

Fig. 9. Plan view--CREWLINE--U7ab.

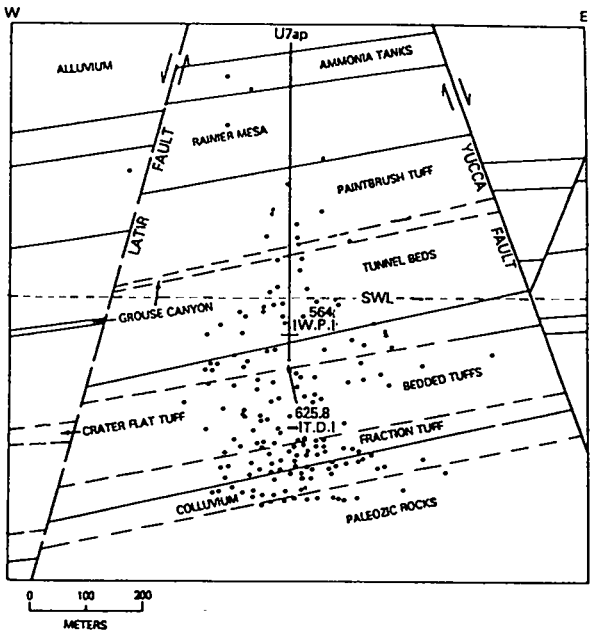

Fig. 10. Cross section--CREWLINE--U7ab.

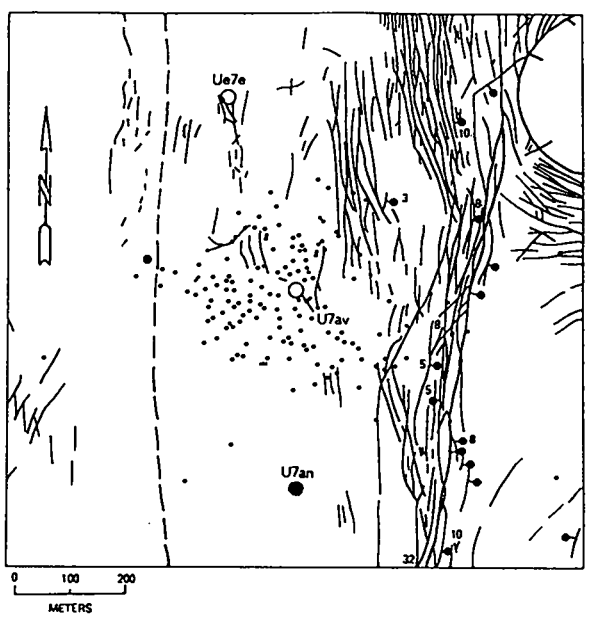

Fig. 11. Plan view--LOWBALL--U7an.

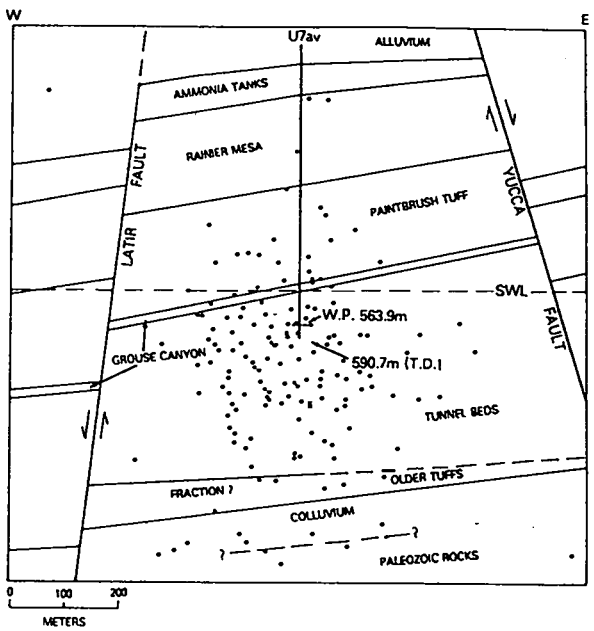

Fig. 12. Cross section--LOWBALL--U7an.

The microquakes associated with displacement along major faults and with surface cracking occur immediately after the detonation of the device. The instrumentation system is saturated at this time and no events can be located.

Microquakes sometimes cluster along structural and stratigraphic interfaces when the detonation is near the interface. For example, microquakes cluster at the Tuff-Paleozoic interface in the U7ap event but not in the U7an, even though they are in the same structural block; the primary difference between the two tests was the scaled distance to the Paleozoic interface.

When a nuclear test is conducted in tuffs, the subsequent microquakes do not cluster at the water table boundary. However, preliminary data from tests conducted in alluvium do show microquake clustering at the water table.

There are two general groups of microquakes in most of the nuclear tests monitored, one group with shallow hypocenters probably associated with the depth of spall and the second, deeper group associated with the stress cage. Most of the microquakes associated with the stress cage occur between three to five cavity radii from the working point.

B. Frequency Distributions of Microquake Activity

The frequency distributions of microquakes radially out from the working point for U7ab, U7an, U7ap, and U7av are shown in Fig. 13. The radii of the cavities created by these nuclear explosions range from 30 m to 50 m, depending on the actual yield. The microquake activity associated with the stress cage is located roughly from one to seven cavity radii from the working point, with the peak activity generally occurring about three cavity radii from the working point. The scaled distance from the nuclear device to the Paleozoic interface is smallest for the U7ap event. The peak activity at U7ap was about five cavity radii instead of the two and one-half to three cavity radii observed on the other tests. Apparently, the interaction of the stress wave from the explosion, with the nearby large impedance mismatch at the Paleozoic interface, caused the increased microquake activity.

The frequency distributions of the microquakes for focal depth for U7ab, U7ap, U7an, and U7av are shown in Fig. 14. The microquake activity reaches a maximum from one cavity radius to three cavity radii below the working point for each event except for U7an, where the maximum activity is less than one cavity radius below the working point. Increased activity is also seen at the Paleozoic interface for events U7ab, U7ap, and U7av. This activity is greater for U7ap where again the scaled distance from the nuclear device to the Paleozoic interface is smaller than the other events. Finally, for U7ab, the activity at about 200 m corresponds to the shallow microquakes located at the Ammonia Tanks pinch out (Fig. 7).

C. Aftershock Magnitudes

The statistical distributions of microquake parameters (for example, frequency of occurrence as a function of magnitude, time, and location) are useful in determining their relationships to nuclear test parameters, such as yield and DOB. The magnitudes used are defined by a formula developed at Los Alamos for use with naturally occurring, local microquakes:

$$M_L = 2.79 \text{ Log } T_{(sec)} - 3.63 \quad ,$$

where T is the duration of the event in seconds measured from the onset of the first P phase to the point in time when the coda is no longer visible above discernible background noise.

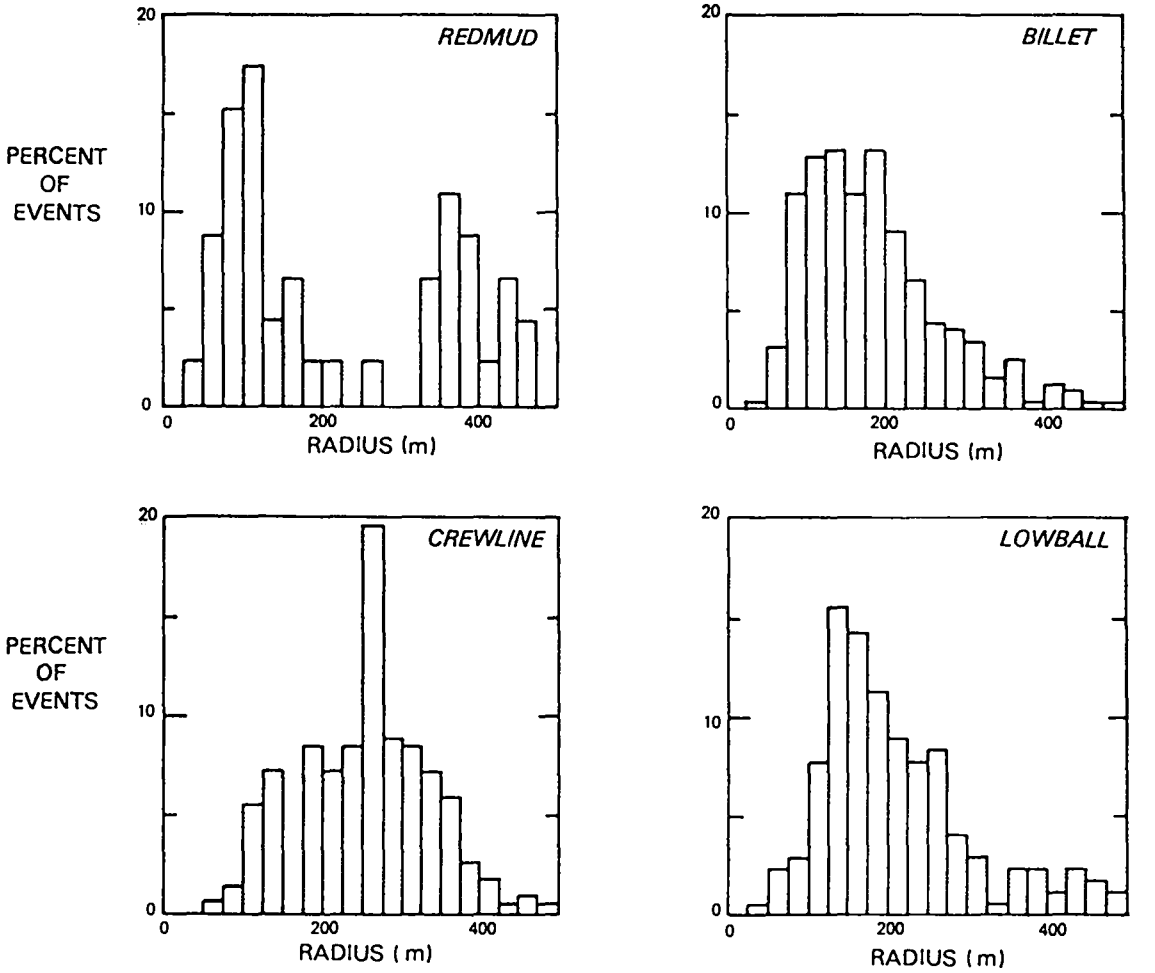

Fig. 13. Frequency plots of radial distance of microquakes from the working point: (a) REDMUD--U7ab; (b) BILLET--U7an; (c) CREWLINE--U7ap; and (d) LOWBALL--U7av.

Figure 15 show the plots of percentages of events in magnitude ranges of 0.25 unit width for the three tests for which microquake durations were available. The frequency peaks at approximately magnitude -1.0 for U7ab, -0.5 for U7an, and +0.7 for U7ap. A hint of a relationship exists between nuclear yield and peak event magnitude. No apparent relationship to DOB or SDOB (scaled depth of burial) has been observed so far.

D. Aftershock Activity as a Function of Time

The underground nuclear tests on which Los Alamos has fielded close-in seismic nets can be arranged into four separate groups based on the time and kind of collapse phenomena: (1) early surface collapse in which a large surface crater (approximately equal in volume to the underground cavity) forms within approximately 2 hours of shot time; (2) late surface collapse in which a large surface sink forms after a few hours to several days after shot time; (3) early partial collapse in which there is cavity collapse and major

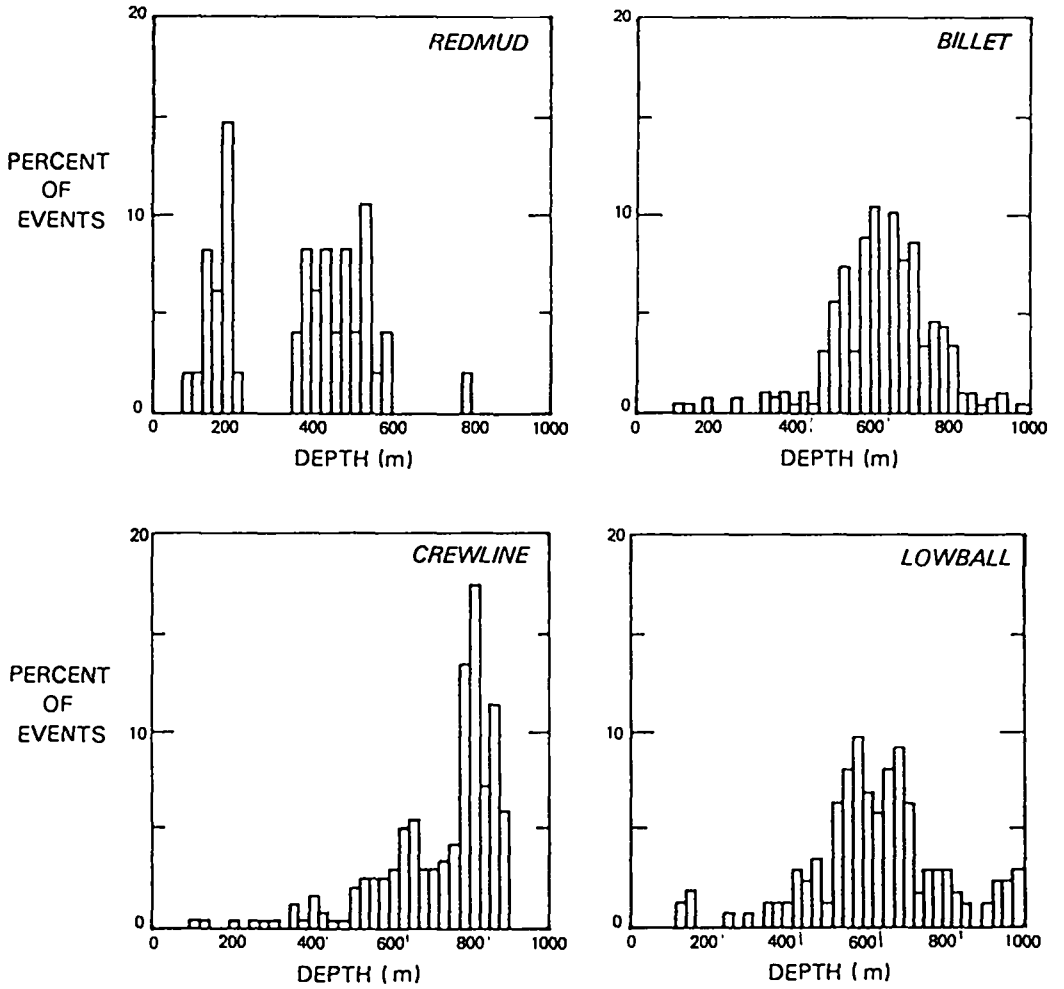

Fig. 14. Frequency plots of depth of microquakes: (a) REDMUD--U7ab; (b) BILLET--U7an; (c) CREWLINE--U7ap; and (d) LOWBALL--U7av.

chimneying within approximately 2 hours of shot time; and (4) late partial collapse in which the cavity collapse and chimneying occur from a few hours to several days after shot time.

The level of seismic activity generally associated with early surface collapse is shown qualitatively in Fig. 16. At shot time the level of activity rises sharply and then decays over a period of several minutes to a level far above the preshot background, so high that the instrumentation records the continuous arrivals from hundreds of microquakes. None of the first arrivals from the smaller individual microquakes can be identified; therefore, no locations were determined for these. A few minutes before surface collapse occurs, there is a sudden increase in seismic activity that peaks at collapse time. The activity then rapidly decreases to near the preshot background level.

The seismic activity level associated with late surface collapse is shown qualitatively in Fig. 16. At shot time, the activity increases instantaneously to its maximum value and then decreases rapidly in a few minutes to

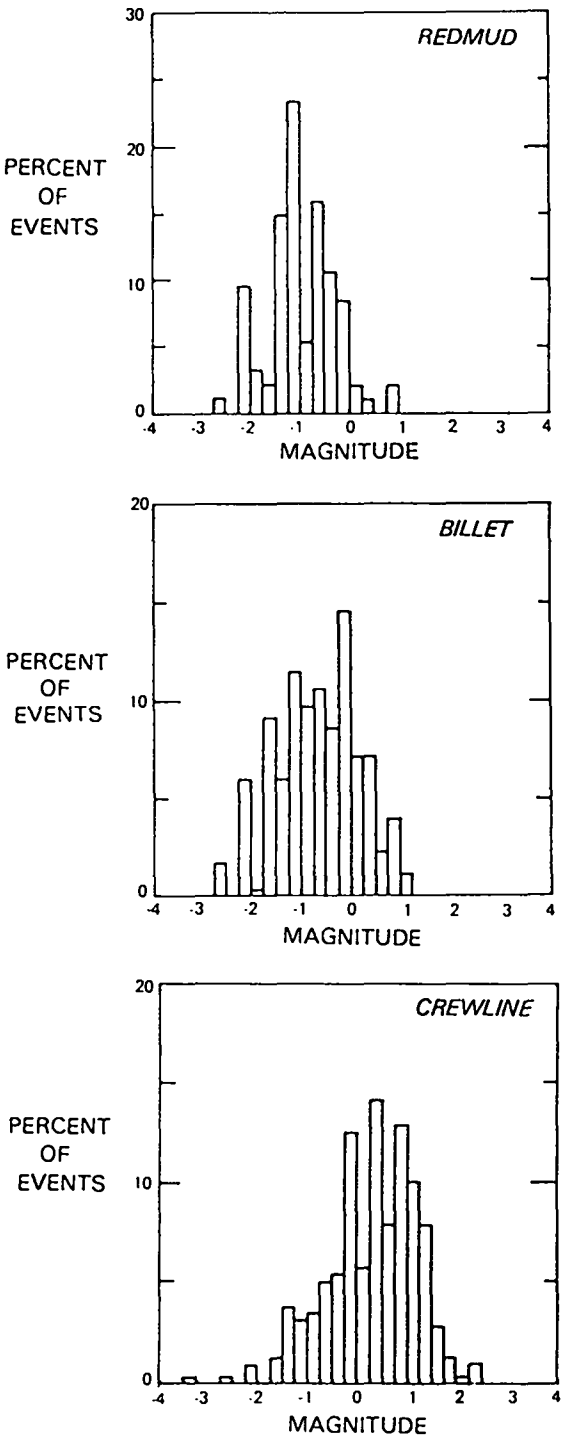

Fig. 15. Magnitude frequency distribution: (a) REDMUD--U7ab; (b) BILLET--U7an; and (c) CREWLINE--U7ap.

a level significantly above the preshot background. Shortly before collapse the activity again increases rapidly, then immediately after collapse it drops rapidly to a level above the preshot background but significantly below the precollapse level. Except for the few minutes at shot time and at collapse, most of the individual microquakes are easily identifiable, and about 20% of these are locatable. We do not have data that show how or over what period of time the aftershock decays to the preshot background after collapse.

The seismic activity associated with the early subsurface collapse exhibited by U7ab is detailed in Fig. 16. At shot time the activity increases instantly to a maximum, then decays in a few minutes to a level that is far above the preshot background with a continuous arrival of signals from hundreds of microquakes--so many that individual microquakes cannot be identified. After partial collapse the activity drops to a level that is above the preshot background, or a few tens of events per hour. Data taken at the site 12 months after U7ab was detonated showed about one microquake per day--still above the preshot background.

The seismic activity associated with the late subsurface collapse exhibited by U7an and U7ap is shown qualitatively in Fig. 16. At shot time the activity increased instantly to a maximum, then decayed in a few minutes to a level of several tens of microquakes per hour. These events are distinct with about 20% being locatable. This activity remained relatively constant over the recording period. About one event per day for a recording period of 15 days was identified. After partial collapse occurred, the activity decreased substantially but still remained above the preshot level. Detonation seismic nets were installed 17 months after U7ap detonation and 12 months after U7an to measure residual activity.

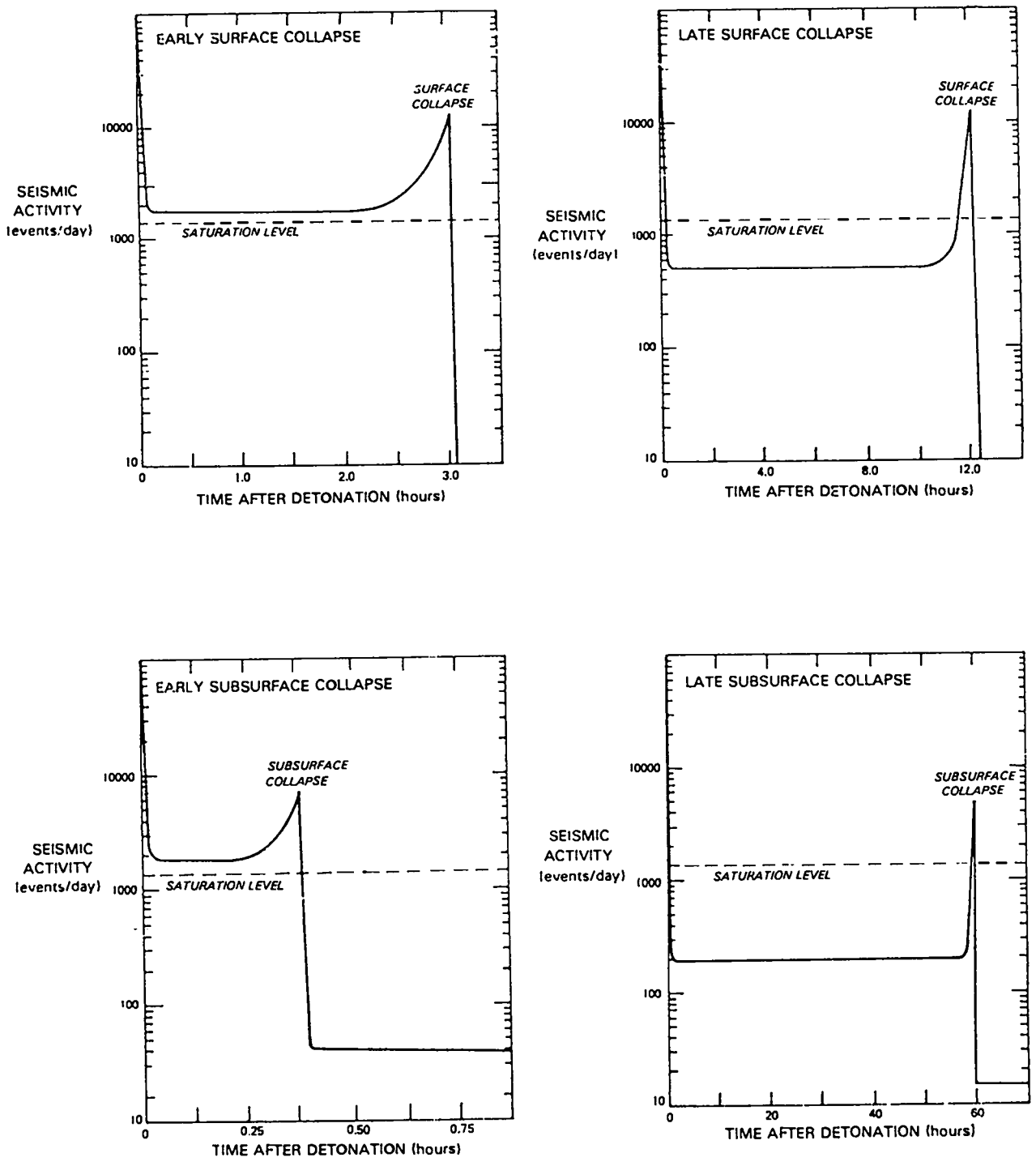

Fig. 16. Seismic activity: (a) early surface collapse; (b) late surface collapse; (c) early subsurface collapse; and (d) late subsurface collapse.

V. ACKNOWLEDGMENTS

The authors gratefully acknowledge the technical support of the Instrumentation, Timing, and Firing Group at Los Alamos and the EG&G, Inc. staff at the Nevada Test Site for their continuing efforts to instrument and record each Los Alamos event. We wish to express our sincere appreciation to Jack House, Containment Project Manager at Los Alamos, for his continued interest and financial support of this effort, without which this project would not have been possible.

REFERENCES

Boucher, G., A. Ryall, and A. E. Jones, Earthquakes Associated with Underground Nuclear Explosions, J. Geophys. Res., Vol. 74, pp. 3808-3820, 1969.

Brune, J. N., and P. W. Pomeroy, Surface Wave Radiation Patterns for Underground Nuclear Explosions and Small-Magnitude Earthquakes, J. Geophys. Res., Vol. 68, pp. 5005-5028, 1963.

Engdahl, E. R., Seismic Effects of the Milrow and Connikin Nuclear Explosions, Bull. Seism. Soc. Am., Vol. 62, pp. 1411-1423, 1972.

Hamilton, R. M., and J. H. Healy, Aftershocks of the Benham Nuclear Explosion, Bull. Seism. Soc. Am., Vol. 59, pp. 2271-2281, 1969.

Hamilton, R. M., F. A. McKeown, and J. H. Healy, Seismic Activity and Faulting Associated with a Large Underground Nuclear Explosion, Science, Vol. 166, pp. 601-604, 1969.

Houser, F. N., Subsidence Related to Underground Nuclear Explosions, Nevada Test Site, Bull. Seism. Soc. Am., Vol. 59, pp. 2231-2251, 1969.

Perret, W. R., Jorum Early Aftershock Measurements, J. Geophys. Res., Vol. 76, pp. 2730-2734, 1971.

Ryall, A., and W. A. Savage, A Comparison of Seismological Effects for the Nevada Underground Test Boxcar with Natural Earthquakes in the Nevada Region, J. Geophys. Res., Vol. 74, pp. 4281-4289, 1969.

Stauder, W., Smaller Aftershocks of the Benham Nuclear Explosion, Bull. Seism. Soc. Am., Vol. 61, pp. 417-428, 1971.

Printed in the United States of America
Available from
National Technical Information Service
US Department of Commerce
5285 Port Royal Road
Springfield, VA 22161

Microfiche (A01)

Page Range	NTIS Price Code	Page Range	NTIS Price Code	Page Range	NTIS Price Code	Page Range	NTIS Price Code
001-025	A02	151-175	A08	301-325	A14	451-475	A20
026-050	A03	176-200	A09	326-350	A15	476-500	A21
051-075	A04	201-225	A10	351-375	A16	501-525	A22
076-100	A05	226-250	A11	376-400	A17	526-550	A23
101-125	A06	251-275	A12	401-425	A18	551-575	A24
126-150	A07	276-300	A13	426-450	A19	576-600	A25
						601-up*	A99

*Contact NTIS for a price quote.

Los Alamos